JCB

Grousl et al., https://doi.org/10.1083/jcb.201708116

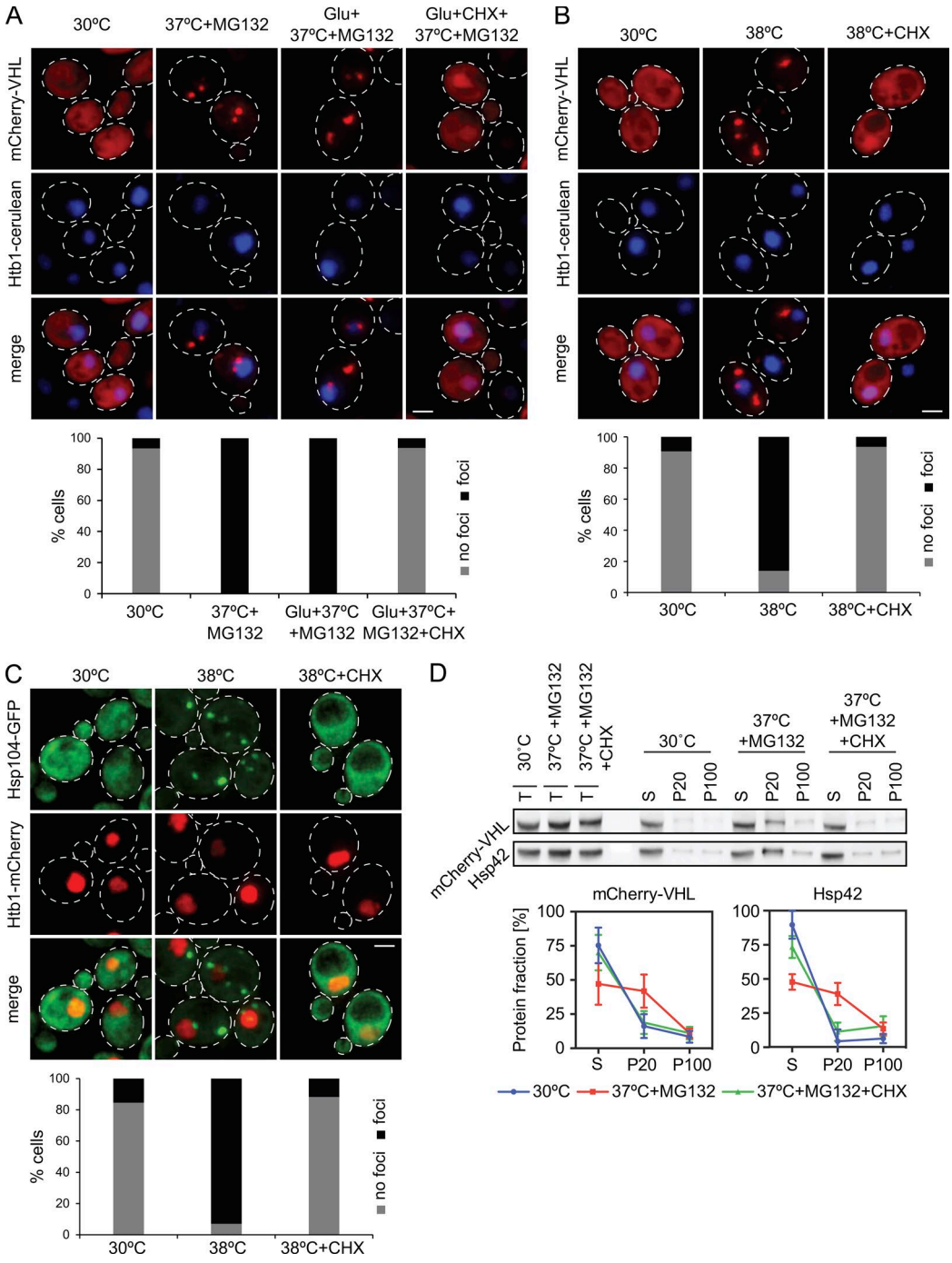

Figure S1. **Protein aggregation depends on translation. (A)** Localization patterns of mCherry-VHL in *S. cerevisiae* cells and their superposition with the nuclear marker Htb1-cerulean upon control conditions (30°C) or proteotoxic stress (37°C for 30 min + MG132) in the absence or presence of CHX. Expression of mCherry-VHL was shut off by preincubation with glucose (Glu) for 30 min if indicated. **(B and C)** Localization patterns of mCherry-VHL (B) or Hsp104-GFP (C) in *S. cerevisiae* cells and their superposition with the nuclear markers Htb1-cerulean/Htb1-mCherry upon control conditions (30°C) or heat stress (38°C) in the absence or presence of CHX. Maximal projection of widefield *z* stack images with corresponding quantifications ($n > 50$ cells) are presented. Bars, 2 µm. **(D)** *S. cerevisiae* cells expressing mCherry-VHL were grown at 30°C and heat shocked (37°C for 30 min + MG132) in the absence or presence of CHX. Total (T), soluble (S), and insoluble (P20 and P100) cell fractions were isolated. The relative fractions (%) of mCherry-VHL and Hsp42 were determined by Western blotting using specific antibodies. Error bars denote SD based on at least three independent experiments.

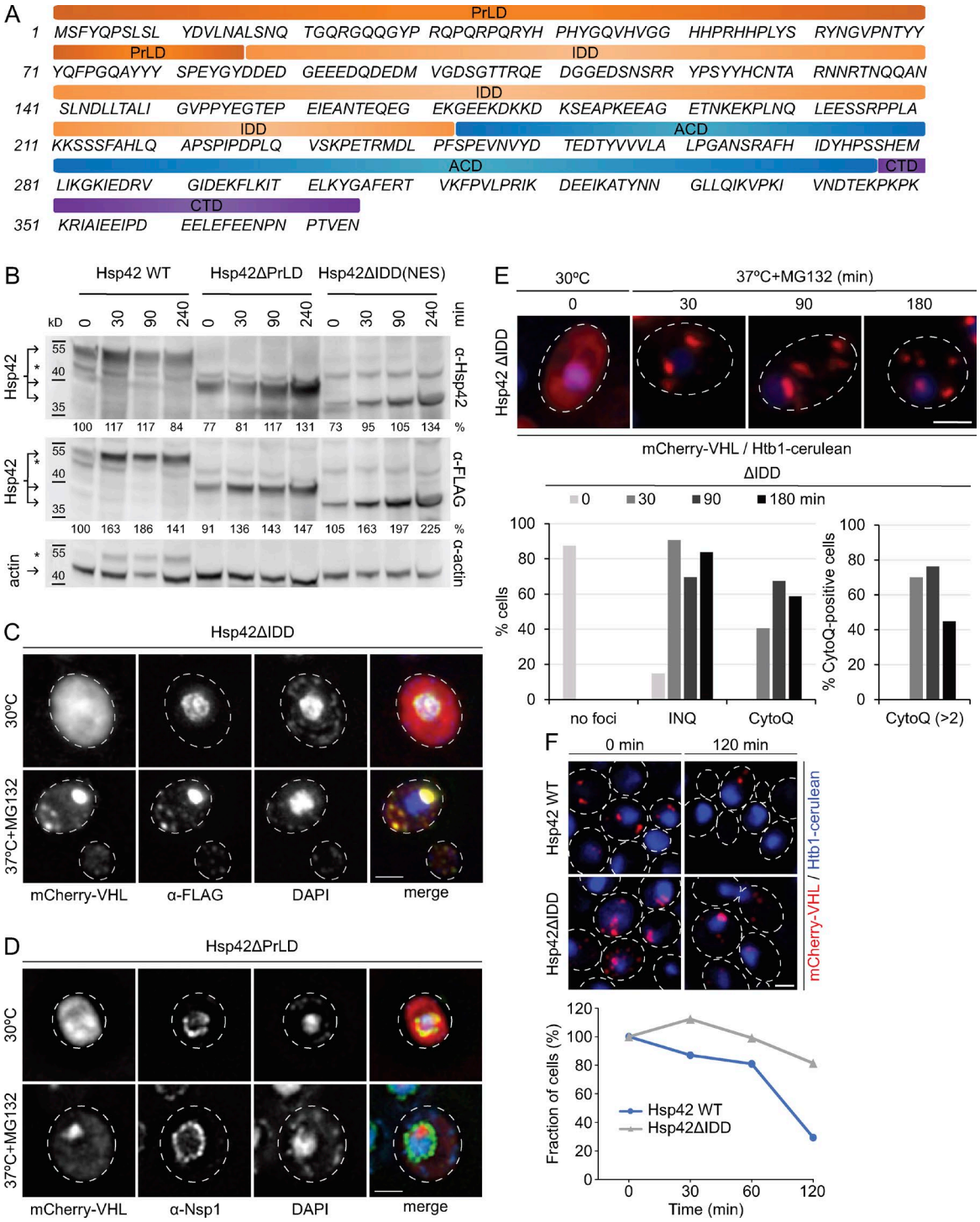

Figure S2. **Analysis of Hsp42 deletion mutants. (A)** Primary sequence of Hsp42. Numbering and Hsp42 domain organization is given. **(B)** Expression levels of Hsp42 WT and deletion mutants were determined before (30°C) and after proteotoxic stress (37°C + MG132) using Hsp42- and FLAG-specific antibodies. The sizes of Hsp42 proteins are indicated (arrows). Asterisks indicate unspecific bands. Actin levels are given as loading controls. Levels of Hsp42 WT and deletion mutants were quantified by ImageJ taking variations of the actin loading control into account. **(C)** Immunofluorescence images of the Hsp42ΔIDD mutant and its superposition with mCherry-VHL and DAPI upon control conditions (30°C) and proteotoxic stress (37°C at 30 min + MG132) are shown. **(D)** Subcellular localization of mCherry-VHL and its superposition with immunofluorescently labeled nuclear envelope marker Nsp1 and DAPI in Hsp42ΔPrLD–expressing yeast cells at the same conditions as in B. **(E)** Localization patterns of mCherry-VHL and their superposition with the nuclear marker Htb1-cerulean in Hsp42ΔIDD–expressing yeast cells upon control conditions (30°C) and proteotoxic stress (37°C + MG132). The number of cells showing CytoQ (mCherry-VHL foci distant from the Htb1-cerulean signal) or INQ (mCherry-VHL foci adjacent or overlapping with the Htb1-cerulean signal) inclusions was quantified at the indicated time points ($n > 50$ cells). **(F)** *S. cerevisiae* expressing either Hsp42 WT or Hsp42ΔIDD and mCherry-VHL were grown at 30°C and exposed to proteotoxic stress (37°C for 180 min + MG132). Afterward, MG132 was removed, and cells were recovered at 30°C. The number of cells harboring mCherry-VHL foci was determined before MG132 removal and at different time points during the recovery phase ($n > 85$ for each time point). Fractions were normalized to the starting value. DNA was stained by Htb1-cerulean. Maximal projections of widefield z stack images are presented. Bars, 2 µm.

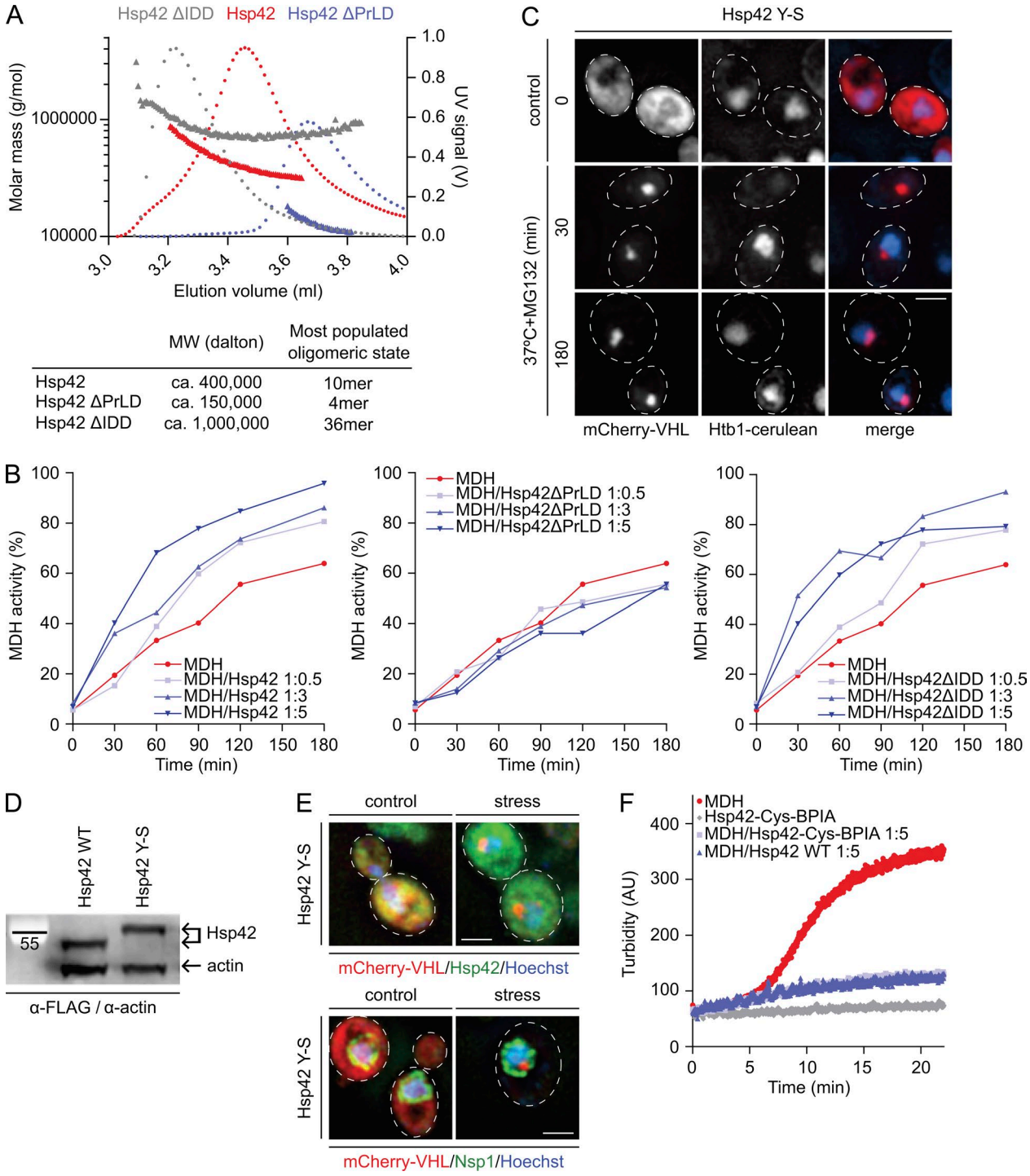

Figure S3. **PrLD is the major Hsp42 substrate interaction site. (A)** PrLD and IDD control Hsp42 oligomerization. Oligomeric states of Hsp42 WT and deletion mutants were determined by static light scattering coupled with size-exclusion chromatography. The UV profiles (right y axis) are shown as dotted lines. Determined molar masses (left y axis) and most populated oligomeric states of the Hsp42 proteins are indicated. **(B)** MDH was denatured for 30 min at 47°C in the absence or presence of Hsp42 WT or deletion mutants at the indicated ratios. MDH refolding from aggregated or Hsp42-complexed states was initiated at 30°C by addition of the yeast-disaggregating bichaperone system (Ssa1, Sis1, Sse1, and Hsp104). The enzymatic activity of native MDH was set at 100%, and the activity of refolded MDH was determined at indicated time points. Representative refolding curves are shown. **(C)** Localization patterns of mCherry-VHL and its superposition with the nuclear marker Htb1-cerulean in *S. cerevisiae* cells expressing the Hsp42-Y/S mutant at 30°C (control) and proteotoxic stress (37°C + MG132) conditions. Representative images are shown. **(D)** Expression levels of Hsp42 WT and Hsp42-Y/S mutants were determined using Hsp42-specific antibody. The positions of Hsp42 proteins are indicated (arrows). Actin levels are given as loading controls. Molecular mass is indicated in kilodaltons. **(E)** Immunofluorescence images of the colocalization pattern of Hsp42-Y/S and mCherry-VHL and their superposition with Hoechst 33342 (top) or the nuclear envelope marker Nsp1 (bottom) at 30°C (control) and proteotoxic stress (37°C for 30 min + MG132). Maximal projections of widefield z stack images are presented. Bars, 2 µm. **(F)** MDH was denatured for 30 min at 47°C in the absence or presence of either Hsp42 WT or BPIA-labeled Hsp42-Cys variant. As a control, Hsp42-Cys-BPIA was heated alone. The formation of MDH aggregates was followed by turbidity measurements.

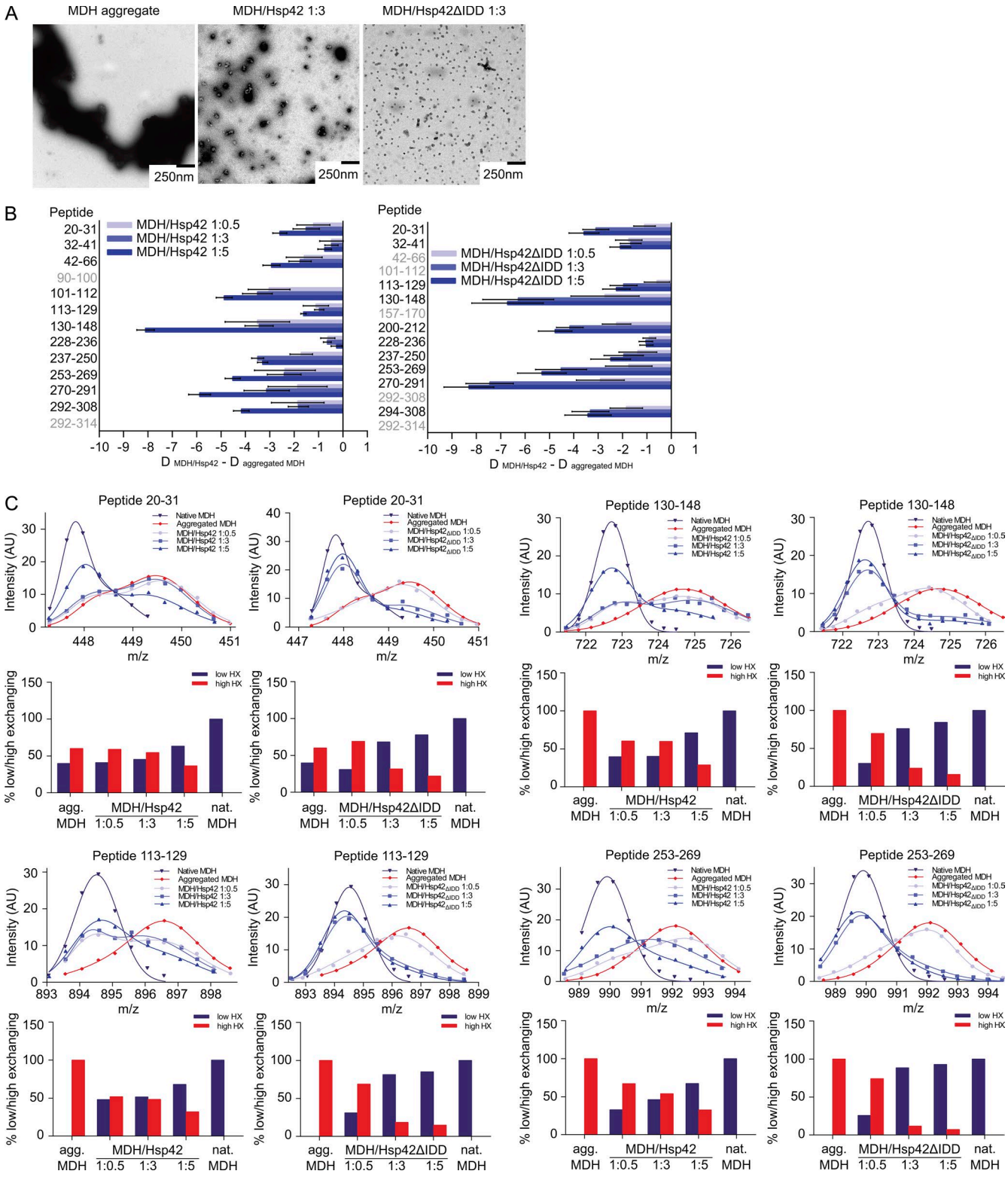

Figure S4. **Hsp42ΔIDD exhibits superior chaperone activity. (A)** Negative-stain electron microscopy pictures of MDH, which was aggregated alone or in the presence of a threefold excess of Hsp42 WT or Hsp42ΔIDD for 30 min at 47°C. **(B)** Difference in deuteron incorporation between heat-induced MDH–Hsp42 WT (left) or MDH–Hsp42ΔIDD (right) complexes and aggregated MDH. Error bars denote SD for each point based on three repetitions. All data were corrected for deuteron losses resulting from back exchange by using a 100% deuterated control. Peptides in grey could not be identified. **(C)** Bimodal distribution of isotope peaks of indicated MDH peptides derived from MDH–Hsp42 (WT or ΔIDD) complexes. Top: intensity versus m/z diagrams for indicated peptic MDH fragments after 30-s HX at 30°C. Bottom: portion of native-like (low HX) and aggregate-like (high HX) populations calculated for respective peptides.

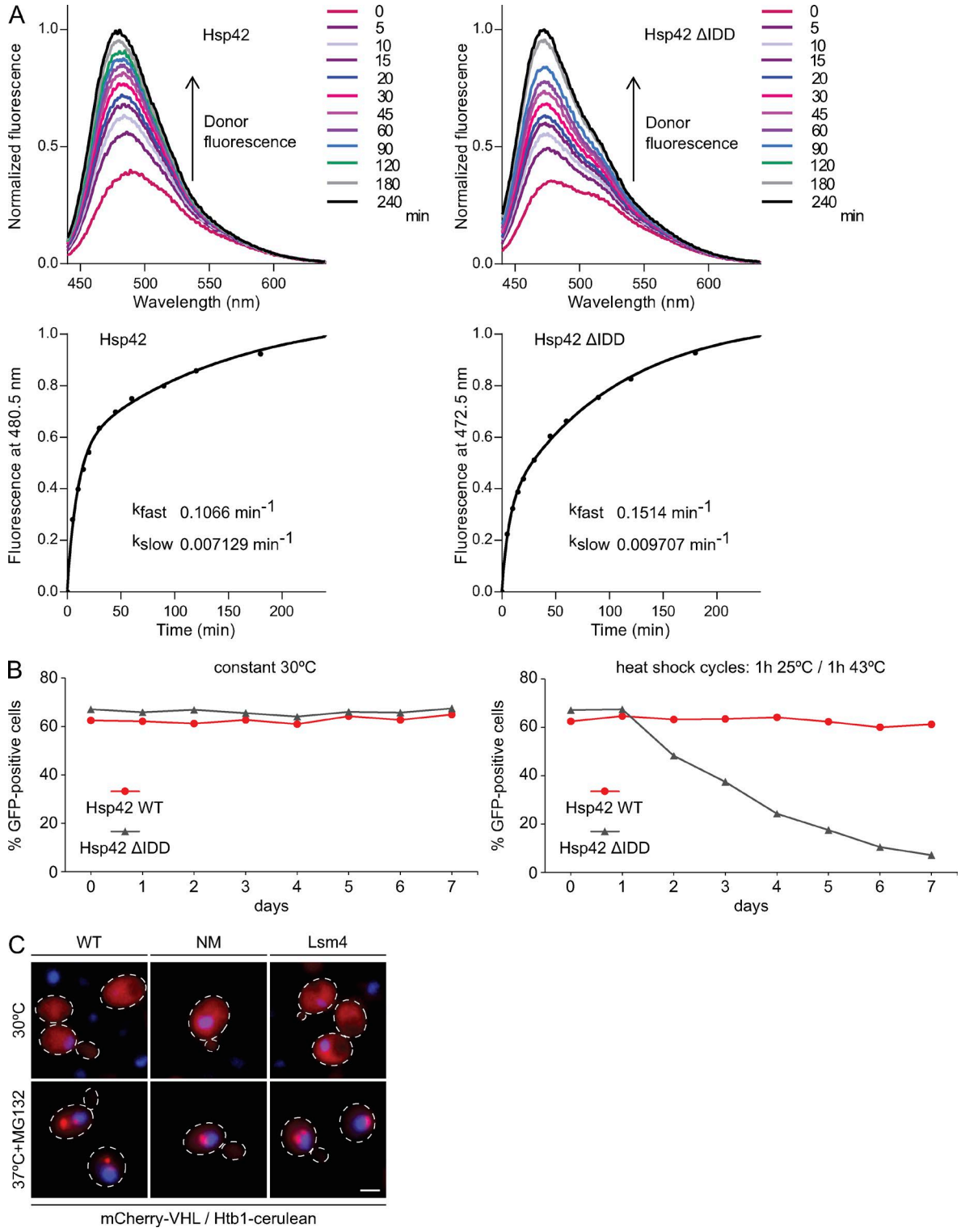

Figure S5. **Subunit exchange kinetics of Hsp42 WT and Hsp42ΔIDD and effects on CytoQ formation and cellular fitness. (A)** Subunit exchange kinetics of Hsp42 WT and Hsp42ΔIDD. The temporal changes in donor fluorescence intensities caused by reversal of FRET upon adding an excess of unlabeled Hsp42 WT or Hsp42ΔIDD to FRET-equilibrated oligomers of both variants labeled with 7-diethylaminocoumarin-3-carboxylic acid and NBD-X are shown (top). Fitting the regain of maximal donor fluorescence (Hsp42 WT, 480.5 nm; Hsp42ΔIDD, 472.5 nm) to FRET-equilibrated oligomers of both variants labeled with 7-diethylaminocoumarin to an exponential two-phase association equation yielded two rates each (bottom). **(B)** Growth competition assays between *S. cerevisiae* cells expressing Hsp42 WT or Hsp42ΔIDD. Fractions of Hsp42 WT and Hsp42ΔIDD–expressing cells in the mixed cultures upon constant growth at 30°C or repetitive heat stress are plotted. The representative result of one out of three biological replicates is shown. **(C)** Canonical prion domains of the yeast prion proteins Sup35 or Lsm4 cannot substitute Hsp42 PrLD in CytoQ formation. Localization patterns of mCherry-VHL and their superposition with the nuclear marker Htb1-cerulean upon control conditions (30°C) and proteotoxic stress (37°C for 30 min + MG132) in Hsp42 WT or Hsp42-NM (NM) and Hsp42-Lsm4 (Lsm4) chimeras. The chimeras harbored prion domains of Sup35 or Lsm4 fused to Hsp42ΔNTE. Maximal projections of representative widefield z stack images are presented. Bar, 2 µm.

Table S1 is a separate Excel file showing a detailed description of yeast strains used in this study.